Tunable Rydberg–Rydberg transitions in helium with reduced sensitivity to dc electric fields by two-colour microwave dressing

OPEN ACCESS
IOP Publishing
Journal of Physics B: Atomic, Molecular and Optical Physics
J. Phys. B: At. Mol. Opt. Phys. **56** (2023) 205001 (9pp)
https://doi.org/10.1088/1361-6455/aceeda

Tunable Rydberg–Rydberg transitions in helium with reduced sensitivity to dc electric fields by two-colour microwave dressing

L L Brown and S D Hogan*

Department of Physics and Astronomy, University College London, Gower Street, London WC1E 6BT, United Kingdom

E-mail: s.hogan@ucl.ac.uk

Received 28 April 2023, revised 4 August 2023
Accepted for publication 9 August 2023
Published 19 September 2023

Abstract

The difference in the static electric dipole polarizabilities of the $1s55s\,^3S_1$ and $1s56s\,^3S_1$ Rydberg levels in helium has been eliminated by dressing the atom with a microwave field near resonant with the single-photon $1s55s\,^3S_1 \rightarrow 1s55p\,^3P_J$ transition. For an $2.82\,\mathrm{mV\,cm^{-1}}$ amplitude dressing field, detuned by $2\pi \times 10\,\mathrm{MHz}$ from the zero-field $1s55s\,^3S_1 \rightarrow 1s55p\,^3P_2$ transition frequency, the dc Stark shift of the two-photon $1s55s\,^3S_1 \rightarrow 1s56s\,^3S_1$ transition between these states remained within $\pm 15\,\mathrm{kHz}$ for electric fields up to $\sim 60\,\mathrm{mV\,cm^{-1}}$. This transition was probed by single-color two-photon microwave spectroscopy, and by two-color two-photon spectroscopy with one strong additional dressing field and a weak probe field. For all measurements, the transition frequencies and Stark shifts were compared, and found to be in excellent quantitative agreement with the results of Floquet calculations of the energy-level structure of the Rydberg states in the presence of the dressing fields and applied dc electric fields. The two-color microwave dressing scheme demonstrated, with one field applied to null the differential polarizability of the Rydberg–Rydberg transition, and the second exploited to allow the two-photon transition to be employed to achieve tunable absorption of single-photons from a weak probe field, will facilitate improved coherence times and tunable single-photon absorption in hybrid cavity QED experiments with Rydberg atoms and superconducting microwave circuits.

Keywords: Rydberg atoms, microwave dressing, microwave spectroscopy

(Some figures may appear in colour only in the online journal)

* Author to whom any correspondence should be addressed.

1. Introduction

Significant advances have occurred recently in the realization of approaches to quantum computation and quantum simulation using arrays of neutral Rydberg atoms [1–3], and superconducting microwave circuits [4, 5]. At present these are two of the leading platforms for quantum information processing, and the implementation of coherent interfaces between them is appealing for many technological applications. The resulting hybrid systems would offer new opportunities for scalability, connectivity, and information storage [6–13].

To implement coherent interfaces between gas-phase atoms in Rydberg states with high principal quantum number n, and solid-state superconducting circuits careful choices of atomic species, quantum states, and circuit design are required, along with exquisite control over the environmental conditions. Helium (He) has been found to be well suited for this work [14–16]. In particular, its low ground-state electric dipole polarizability leads to minimal adsorption on the cryogenically cooled surfaces of superconducting chips, and minimizes the generation of stray electric fields if adsorption does occur. This feature played a key role in the first realization of a coherent interface between Rydberg atoms and microwave fields in superconducting coplanar waveguide (CPW) resonators [16]. In that work, stray dc electric fields were reduced to below $30\,\mathrm{mV\,cm^{-1}}$ at a distance of $\sim 300\,\mu$m above a superconducting niobium nitride (NbN) chip operated at 3.8 K [17].

To maximize atom-resonator coupling at this type of hybrid quantum interface and move toward the single-photon strong-coupling regime, it is desirable to minimize the distance of the atoms from the CPW resonator structures and hence the superconducting chip surfaces. However, in close proximity to cryogenically cooled surfaces, it remains challenging to completely cancel stray electric fields [15, 17–20]. Residual uncancelled inhomogeneous electric fields ultimately cause dephasing and limit coherence times. Therefore, in addition to choosing Rydberg–Rydberg transitions with low sensitivity to these fields [16, 20, 21], it is desirable to engineer the corresponding states to further minimize dc Stark shifts. This quantum state engineering can, for example, be achieved by dressing an atom with appropriate off-resonant radio-frequency or microwave fields as proposed, and subsequently demonstrated in experiments with rubidium atoms for a range of Rydberg states [22–25]. Here, we extend this methodology to experiments with He atoms in low-ℓ (ℓ is the orbital angular momentum quantum number of the Rydberg electron) triplet Rydberg states. The states studied are the same as those successfully used in the implementation of hybrid interfaces with $\lambda/4$ NbN superconducting CPW resonators [16, 17, 26]. We also show that the use of one strong microwave field to null the differential polarizability of the pair Rydberg states between which a two-photon transition is driven, i.e. a 'nulling' field, and a second strong dressing field that supplies one of the photons required to drive this as a two-color transition (this is referred to in the following as the 'control' field), allows tunable absorption of single photons from a weak probe field with minimal sensitivity to residual stray electric fields.

In the following, the microwave dressing schemes implemented in the experiments are first described in section 2 along with the methods used to calculate the effects of these fields, and additional dc electric fields on the atomic energy-level structure. In section 3 the experimental apparatus is presented. The results of the experiments, and their comparison with the results of the calculations, are then discussed in section 4. Finally, in section 5 conclusions are drawn.

2. Microwave dressing schemes

As seen in figure 1, the $1s55s\,^3S_1$ ($|55s\rangle$) and $1s56s\,^3S_1$ ($|56s\rangle$) Rydberg levels in He have weak quadratic Stark shifts. Atoms in these levels can be prepared by resonance-enhanced two-color two-photon laser excitation from the metastable $1s2s\,^3S_1$ level [27], and can be efficiently and selectively detected by pulsed electric field ionization [26]. Together, these features make them well suited for use in coherent interfaces with superconducting microwave circuits [16, 17, 26]. The transition between these Rydberg states can be driven as a single-color two-photon transition at an angular frequency $\omega_{55s,56s}/2 = 2\pi \times 19.556\,499\,\mathrm{GHz}$ in the absence of external fields. Since the static electric dipole polarizabilities, α_{ns}, of the $|55s\rangle$ and $|56s\rangle$ states are similar ($\alpha_{55s} = 2.058\,\mathrm{GHz\,(V\,cm^{-1})^{-2}}$ and $\alpha_{56s} = 2.334\,\mathrm{GHz\,(V\,cm^{-1})^{-2}}$), the differential polarizability, that affects the Stark shift of the $|55s\rangle \rightarrow |56s\rangle$ transition, is $\alpha_{55s,56s} = 0.276\,\mathrm{GHz\,(V\,cm^{-1})^{-2}}$. Consequently, the Stark shift of the single-color two-photon transition, with respect to the frequency of the individual photons, $\omega_{55s,56s}/2$, are $<1\,$MHz in dc electric fields $<100\,\mathrm{mV\,cm^{-1}}$ [16].

In the following, we demonstrate that the sensitivity of the two-photon $|55s\rangle \rightarrow |56s\rangle$ transition to dc electric fields can be significantly reduced by engineering the atomic energy-level structure using appropriate off-resonant microwave dressing fields. These fields are detuned from the single-photon $1s55s\,^3S_1 \rightarrow 1s55p\,^3P_J$ ($|55s\rangle \rightarrow |55p\rangle$) electric-dipole transition at $\omega_{55s,55p} = 2\pi \times 9.118\,568\,\mathrm{GHz}$ (see figure 1). They therefore admix $|55p\rangle$ character into the $|55s\rangle$ state to 'null' the differential polarizability of the $|55s\rangle \rightarrow |56s\rangle$ transition.

To determine amplitudes and detunings of nulling microwave fields that minimize the sensitivity of the $|55s\rangle \rightarrow |56s\rangle$ transition to dc electric fields, calculations of the Stark shifts of the Rydberg states were performed using the Floquet method and matrix diagonalization [28–30]. In this treatment, a dc electric field $\vec{F}_{\mathrm{dc}} = (0, 0, F_{\mathrm{dc}})$ acting in the z dimension, and the nulling microwave field, polarized linearly also in the z dimension, i.e. $\vec{F}_{\mathrm{null}} = [0, 0, F_{\mathrm{null}} \cos(\omega_{\mathrm{null}} t)]$ and with an angular frequency, ω_{null}, were considered (Note: the coordinate system used when referring to the geometry of the experimental apparatus is indicated in figure 2). Within the electric dipole approximation, the Hamiltonian describing the interaction of the atom with these fields can be expressed as

$$H(t) = H_0 + eF_{\mathrm{dc}}\, z + eF_{\mathrm{null}} \cos(\omega_{\mathrm{null}} t)\, z, \qquad (1)$$

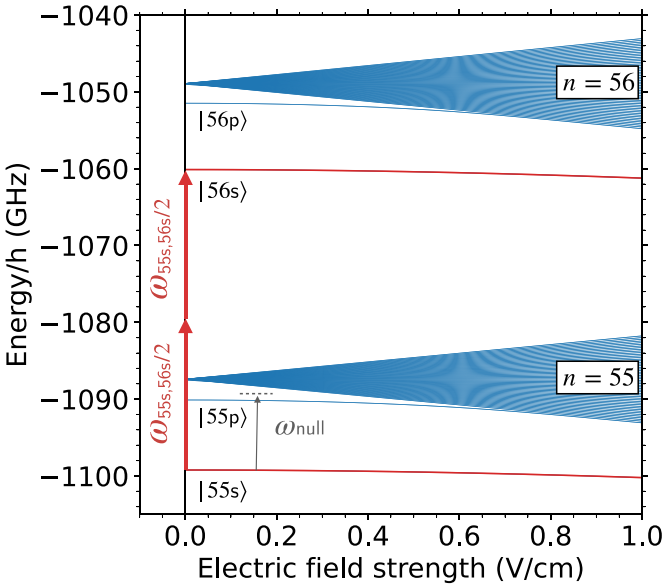

Figure 1. Energy-level diagram of triplet Rydberg states in He with $m_\ell = 0$. The single-color two-photon $|55s\rangle \rightarrow |56s\rangle$ transition discussed in the text is indicated by the thick vertical red arrows. The nulling field, with an angular frequency $\omega_{\rm null}$, was positively detuned from the $|55s\rangle \rightarrow |55p\rangle$ transition, as indicated by the thin grey arrow (see text for details).

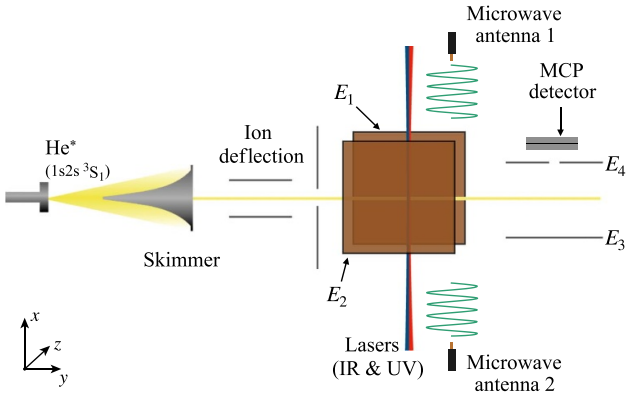

Figure 2. Schematic diagram of the experimental apparatus. The microwave antennas were positioned outside the vacuum chamber.

where H_0 is the field-free Hamiltonian, z is the position of the electron with respect to the nucleus, and the periodicity of $H(t)$ is governed by the frequency of the microwave field, $\omega_{\rm null}$. Using the Floquet theorem, the time-dependent Schrödinger equation associated with this time-periodic Hamiltonian can be transformed into a time-independent eigenvalue problem by choosing a basis in which the Fourier components of the periodic perturbation are accounted for [29]. The Fourier components, denoted by the integer $q_{\rm null}$, are included as sidebands on each unperturbed basis state. This results in an enlarged basis in which each Rydberg state with $q_{\rm null} = 0$ has associated with it an infinite set of sidebands, $q_{\rm null} = \pm 1, \pm 2, \ldots$, offset by energies $q_{\rm null}\hbar\omega_{\rm null}$.

After this transformation, the time-independent Hamiltonian, $H^{'}$, can be expressed in matrix form in the $|n\,\ell\,m_\ell\,q_{\rm null}\rangle$ basis, where m_ℓ is the azimuthal quantum number. In this basis, when $F_{\rm dc} = F_{\rm null} = 0$, the matrix is diagonal, and

$$\langle n\,\ell\,m_\ell\,q_{\rm null}|H'|n\,\ell\,m_\ell\,q_{\rm null}\rangle = E_{n\ell} + q_{\rm null}\hbar\omega_{\rm null}. \quad (2)$$

The field-free energies of the Rydberg states, $E_{n\ell} = hcR_{\rm He}/(n-\delta_{n\ell})^2$, were calculated using the quantum defects, $\delta_{n\ell}$, listed in table 1 [31], and the Rydberg constant, $R_{\rm He}$, corrected for the reduced mass of He.

Table 1. Quantum defects of low-ℓ $n = 55$ and $n = 56$ triplet Rydberg states in He [31].

ℓ	$\delta_{55\,\ell}$	$\delta_{56\,\ell}$
0	0.296 669	0.296 669
1	0.068 354	0.068 354
2	0.002 889	0.002 889
3	0.000 447	0.000 447

The matrix elements representing the interaction with the time independent dc electric field were expressed in spherical polar coordinates such that

$$\langle n'\,\ell'\,m'_\ell\,q'_{\rm null}|eF_{\rm dc}z|n\,\ell\,m_\ell\,q_{\rm null}\rangle = eF_{\rm dc}\langle \ell'\,m'_\ell|\cos\theta|\ell\,m_\ell\rangle \times \langle n'\,\ell'|r|n\,\ell\rangle\delta_{q_{\rm null},\,q'_{\rm null}}. \quad (3)$$

This dc field couples states of the same sideband order, i.e. $\delta_{q_{\rm null},\,q'_{\rm null}}$. The angular integrals in equation (3) were calculated using the analytic expressions [28],

$$\langle \ell\,m_\ell|\cos\theta|(\ell-1)\,m_\ell\rangle = \sqrt{\frac{\ell^2 - m_\ell^2}{(2\ell+1)(2\ell-1)}}, \quad (4)$$

$$\langle \ell\,m_\ell|\cos\theta|(\ell+1)\,m_\ell\rangle = \sqrt{\frac{(\ell+1)^2 - m_\ell^2}{(2\ell+3)(2\ell+1)}}. \quad (5)$$

These impose the restriction that the matrix elements are zero unless $m'_\ell = m_\ell$ and $\ell' = \ell \pm 1$. The radial integrals in equation (3) were calculated using the Numerov method with a pure Coulomb potential [28, 32].

The matrix elements associated with the nulling field in equation (1) were also transformed into spherical polar coordinates and calculated using the same methods as the dc field components. However, in this case the off-diagonal elements couple Fourier components for which $\Delta q_{\rm null} = \pm 1$ such that,

$$\langle n'\,\ell'\,m'_\ell\,q'_{\rm null}|eF_{\rm null}\cos(\omega_{\rm null}t)z|n\,\ell\,m_\ell\,q_{\rm null}\rangle \equiv \frac{eF_{\rm null}}{2}\langle \ell'\,m'_\ell|\cos\theta|\ell\,m_\ell\rangle\langle n'\,\ell'|r|n\,\ell\rangle\,\delta_{q_{\rm null}\pm 1,\,q'_{\rm null}}. \quad (6)$$

Using this approach, the effect of the nulling microwave field on the energy-level structure of the atom can be determined from the eigenvalues of the resulting Hamiltonian matrix. To achieve convergence of the numerical results, at $n = 55$ and $n = 56$ for $\omega_{\rm null} \simeq 2\pi \times 9$ GHz, states with $52 \leqslant n \leqslant 58$, all allowed values of ℓ, and Fourier components for which $q_{\rm null} \leqslant |2|$ were included in the calculations.

To calculate the combined effect of the strong off-resonant nulling, and control microwave fields that allow the $|55s\rangle \rightarrow |56s\rangle$ transition to be driven as a two-color two-photon transition with single-photon absorption from the weak probe field, the Floquet calculations were extended through a multi-frequency Fourier expansion [33, 34]. In this process, the computational basis was enlarged to include additional Fourier components associated with the dressing field $\vec{F}_{\rm ctl} = [0, 0, F_{\rm ctl}\cos(\omega_{\rm ctl}\, t)]$ with angular frequency $\omega_{\rm ctl}$ and amplitude $F_{\rm ctl}$. In the resulting $|n\,\ell\, m_\ell\, q_{\rm null}\, q_{\rm ctl}\rangle$ basis, $q_{\rm ctl}$ represents the sideband order of the control field. In this case, the diagonal matrix elements of the time-independent Hamiltonian $H^{'}$ had the form

$$\begin{aligned}\langle n\,\ell\, m_\ell\, q_{\rm null}\, q_{\rm ctl}|H'|n\,\ell\, m_\ell\, q_{\rm null}\, q_{\rm ctl}\rangle \\ = E_{n\ell} + \hbar\,(q_{\rm null}\,\omega_{\rm null} + q_{\rm ctl}\,\omega_{\rm ctl}).\end{aligned} \tag{7}$$

By analogy with the single-color situation described above the control field couples basis states when $\Delta q_{\rm ctrl} = \pm 1$ while $\Delta q_{\rm null} = 0$, and the nulling field couples basis states when $\Delta q_{\rm null} = \pm 1$ while $\Delta q_{\rm ctrl} = 0$. For $\omega_{\rm null} \simeq 2\pi \times 9\,$GHz and $\omega_{\rm ctl} \simeq 2\pi \times 19.2\,$GHz and dc electric fields up to $\sim$100 mV cm^{-1}, convergence was reached in the calculations when Fourier components of both fields with $q_{\rm null} = q_{\rm ctl} \leqslant |2|$ were included.

3. Experiment

A schematic diagram of the apparatus used in the experiments is presented in figure 2. A pulsed valve, operated at a repetition rate of 25 Hz, released a supersonic beam of He atoms into a vacuum chamber. The atoms in the beam had a mean longitudinal speed of $\sim$1750 m s^{-1}. A dc electric discharge at the exit of the valve was used to populate the metastable $1s2s\,^3S_1$ level [35]. The beam then passed through a 2 mm-diameter skimmer that collimated it, and charged particles produced in the discharge were removed by electrostatic deflection. The atoms then entered the spectroscopy region between the two parallel copper electrodes, E_1 and E_2, which were separated in the z dimension by 1.35 cm. In this region, the atomic beam was intersected by co-propagating continuous wave laser beams used to drive the two-color two-photon $1s2s\,^3S_1 \rightarrow 1s3p\,^3P_2 \rightarrow 1s55s\,^3S_1$ excitation scheme [27]. The first step in this excitation scheme required radiation in the ultraviolet (UV) region of the electromagnetic spectrum at a wavelength of 388.975 nm. The second step was driven in the infrared (IR) at 786.817 nm. The second laser frequency was tuned slightly off-resonance from the field-free transition to the $1s55s\,^3S_1$ level. This allowed short ($\sim$4 mm-long) bunches of excited Rydberg atoms to be prepared using a 2 μs-duration pulsed excitation electric field of $\sim$300 mV cm^{-1}. This was generated by applying a pulsed potential to E_1, to Stark shift the $1s3p\,^3P_2 \rightarrow 1s55s\,^3S_1$ transition into resonance with the frequency stabilized IR laser.

After laser photoexcitation pulsed microwave fields with durations of $T_\mu = 1$, or 3 μs were applied to probe the $|55s\rangle \rightarrow |56s\rangle$ transition. This was driven as a single-color two-photon transition at frequencies close to $\omega_{55s,56s}/2 = 2\pi \times 19.556\,499\,$GHz, or as a two-color two-photon transition with a weak probe field at an angular frequency close to $\omega_{55s,56s}/2 + 300\,$MHz in the presence of a strong control field detuned by $-300\,$MHz from $\omega_{55s,56s}/2$. In general, the intensities of the microwave fields were set to ensure that at most half of the population was transferred from the $|55s\rangle$ state to the $|56s\rangle$ state, i.e. the effective two-photon Rabi frequency was $<2\pi \times 80\,$kHz. Under these conditions, the ac Stark shift of the single-color two-photon $|55s\rangle \rightarrow |56s\rangle$ transition with respect to $\omega_{\rm osc}/2$, induced by this field was $\sim +1\,$kHz.

The dc Stark shifts of the $|55s\rangle \rightarrow |56s\rangle$ transition were measured by applying offset potentials, $V_{\rm off}$, to E_1. Pulsed nulling microwave fields were introduced at the same time as the probe and control fields to engineer the electric dipole polarizability of the $|55s\rangle$ state. The nulling field entered the spectroscopy region of the apparatus from antenna 2 on the opposite side of the atomic beam to the probe and control fields. These were coupled into a single coaxial cable outside the vacuum chamber using a power combiner, and propagated into the chamber from antenna 1. The separation between E_1 and E_2 was less than half the wavelength of the microwave fields used in the experiments. This ensured that all three microwave fields were linearly polarized parallel to the applied dc electric fields. After the microwave and electric field pulses were switched off, the atoms travelled into the region between electrodes E_3 and E_4 where state-selective pulsed electric field ionization was implemented. The resulting electrons were collected at a microchannel plate (MCP) detector to allow the Rydberg state populations to be determined [26].

4. Results

4.1. dc Stark shifts in the presence of nulling fields

To study the effect of differential-polarizability-nulling microwave fields on the dc Stark shift of the $|55s\rangle \rightarrow |56s\rangle$ transition, single-color two-photon microwave spectroscopy was first performed with microwave pulses for which $T_\mu = 3\,\mu$s, and offset electric potentials of up to $|V_{\rm off}| = 120\,$mV applied to E_1, i.e. electric fields up to 89 mV cm^{-1}. When recording these spectra, presented in figure 3, population transfer to the $|56s\rangle$ state was monitored. In this figure, each spectrum is normalized and vertically offset by an amount reflecting the value of $V_{\rm off}$. The Stark shifts observed without the application of a microwave dressing field are displayed in figure 3(a). For $V_{\rm off} = 0\,$V the transition frequency was measured to be 19 556.517 $\pm$ 0.003 MHz (dashed vertical line) with a full-width-at-half-maximum (FWHM) of $\simeq$140 kHz. This FWHM corresponds to the Fourier transform of the $T_\mu = 3-\mu$s-duration microwave pulses at the two-photon level, i.e. at the frequency $\omega_{55s,56s}/2$. This spectral width increased for larger values of $V_{\rm off}$ because the $|ns\rangle$ Rydberg states are more strongly polarized in the resulting fields and consequently more sensitive to electric field fluctuations.

In figure 3(b), a nulling microwave field was applied at a frequency $\omega_{\rm null} = 2\pi \times 9.123\,568\,$GHz. This was detuned by $\Delta_{\rm null} = \omega_{\rm null} - \omega_{55s,55p} = +2\pi \times 5\,$MHz from the field-free $|55s\rangle \rightarrow |55p\rangle$ transition frequency. The amplitude, $F_{\rm null}$,

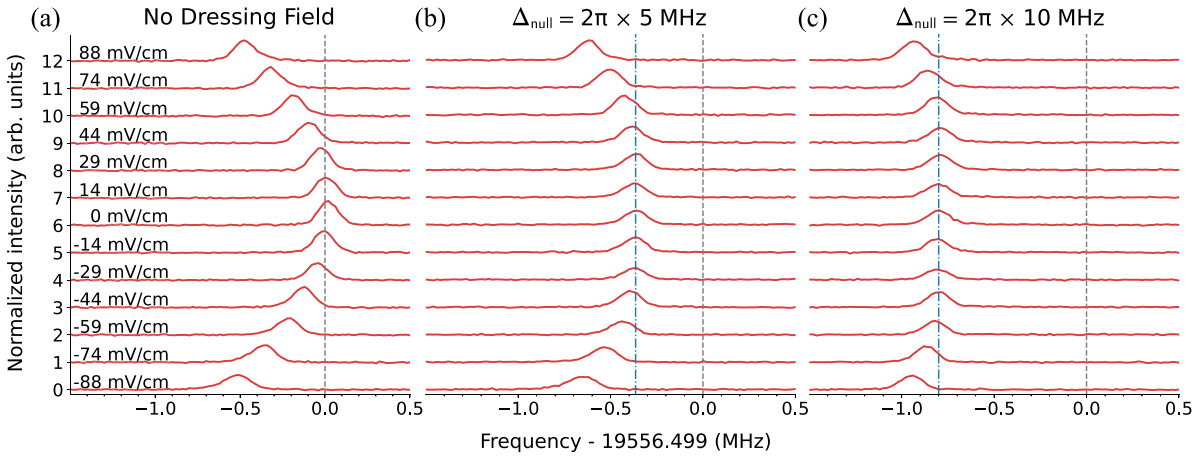

Figure 3. Stark shifts of the single-color two-photon $|55s\rangle \rightarrow |56s\rangle$ transition in (a) the absence of a nulling field, and in the presence of differential-polarizability-nulling microwave fields with detunings of (b) $\Delta_{null} = +2\pi \times 5$ MHz, and (c) $\Delta_{null} = +2\pi \times 10$ MHz from the field-free $|55s\rangle \rightarrow |55p\rangle$ transition frequency. The dashed vertical line in each panel indicates the field free transition frequency. The dash-dotted lines in (b) and (c) indicate the ac-Stark-shifted transition frequencies in zero dc field. The values of V_{off} applied to generate fields up to $\sim$90 mV cm^{-1} in increments of 14.8 mV cm^{-1} when recording each set of data are indicated on the left in panel (a).

of this nulling field was optimized in the experiments to maximize the range of dc fields over which the differential polarizability of the $|55s\rangle$ and $|56s\rangle$ states was minimized. The application of this field resulted in an ac stark shift of the two-photon $|55s\rangle \rightarrow |56s\rangle$ transition of -383 kHz (difference between the dashed-dotted and dashed vertical lines). The value of F_{null} was subsequently determined to be 1.35 mV cm^{-1} by comparison of the measured ac Stark shift in zero dc field, with the results of the Floquet calculations. The reduction in the differential polarizability of the $|55s\rangle$ and $|56s\rangle$ states is evident in the spectra in figure 3(b) from the larger range of offset potentials, in this case up to approximately $\pm$60 mV ($\simeq \pm$ 45 mV cm^{-1}), over which the measured two-photon transition frequency remains within the zero-dc-field resonance width than is the case in panel (a). The nulling field applied when recording the data in figure 3(c) had a larger detuning of $\Delta_{null} = +2\pi \times 10$ MHz and a larger amplitude. The amplitude was again optimized in the experiments and subsequently determined from the calculations to be $F_{null} = 2.82$ mV cm^{-1}. This resulted in an ac Stark shift of -818 kHz in zero dc field, and a further reduction in the sensitivity of the $|55s\rangle \rightarrow |56s\rangle$ transition to dc electric fields. In this case, the measured resonance frequency lies within the zero-dc-field resonance width for values of V_{off} up to approximately $\pm$80 mV ($\simeq \pm$60 mV cm^{-1}).

A more quantitative description of the effect of the nulling microwave field on the single-color two-photon $|55s\rangle \rightarrow |56s\rangle$ transition is presented in figure 4. The dc electric field strength on the horizontal axis in this figure was calculated from the corresponding value of V_{off}, the potential required to minimize stray fields (-3 mV) and the separation of 1.35 cm between E_1 and E_2. The measured resonance frequencies (points) are compared to the results of the Floquet calculations described in section 2 (continuous curves). When comparing the measurements of the Stark shifts to the results of the calculations without the application of the dressing field (uppermost

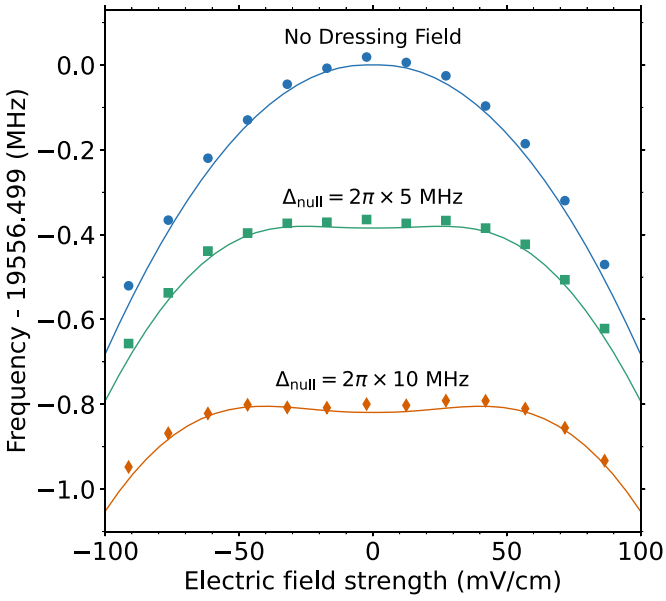

Figure 4. Stark shifts of the single-color two-photon $|55s\rangle \rightarrow |56s\rangle$ transition frequency measured for nulling microwave fields with the detunings, Δ_{null}, indicated (points). The continuous curves associated with each dataset represent the results of Floquet calculations (see text for details).

data set) there is a frequency shift of $\sim$18 kHz. This, and the corresponding shifts in the lower datasets, are attributed to a Doppler shift of the microwave field in the apparatus.

Using the Floquet method to calculate the effect of a nulling field with a detuning $\Delta_{null} = +2\pi \times 5$ MHz from the $|55s\rangle \rightarrow |55p\rangle$ transition, and an amplitude $F_{null} = 1.35$ mV cm^{-1}, the Stark shift of the $|55s\rangle \rightarrow |56s\rangle$ transition was found to remain within $\pm$15 kHz for fields up to $F_{dc} = 45$ mV cm^{-1}. For $\Delta_{null} = +2\pi \times 10$ MHz and $F_{null} = 2.82$ mV cm^{-1}, more effective nulling of the differential polarizability of the $|55s\rangle$ and $|56s\rangle$ states was achieved, with the dc Stark shifts

remaining within $\pm 15\,\mathrm{kHz}$ for fields up to $F_{\mathrm{dc}} = 60\,\mathrm{mV\,cm^{-1}}$. The bound on the minimum achievable dc Stark shift over the largest possible range of field strengths is set by the field strength for which the derivative of the dc Stark shift in the presence of the dressing field changes sign. For example, for $\Delta_{\mathrm{null}} = +2\pi \times 10\,\mathrm{MHz}$ and $F_{\mathrm{null}} = 2.82\,\mathrm{mV\,cm^{-1}}$, there is a Stark shift of $+15\,\mathrm{kHz}$ at this turning point which occurs at $F_{\mathrm{dc}} = 39\,\mathrm{mV\,cm^{-1}}$.

4.2. Resonant Rabi frequency in the presence of dc and nulling fields

The effect of the nulling microwave field on the Rabi frequency of the two-photon $|55\mathrm{s}\rangle \rightarrow |56\mathrm{s}\rangle$ transition for a fixed probe field amplitude was studied to shed light on effects of dephasing on the coherent manipulation of the atoms in the presence of the nulling fields. Measurements of resonant Rabi frequencies were made for dc electric field strengths up to $F_{\mathrm{dc}} = 74\,\mathrm{mV\,cm^{-1}}$ while a nulling field with a detuning $\Delta_{\mathrm{null}} = +2\pi \times 10\,\mathrm{MHz}$ and amplitude $F_{\mathrm{null}} = 2.82\,\mathrm{mV\,cm^{-1}}$ was applied. The results of these measurements are presented in figure 5. For the range of dc fields over which the dressing field was effective at differential polarizability nulling, i.e. $F_{\mathrm{dc}} \lesssim 60\,\mathrm{mV\,cm^{-1}}$, the Rabi frequency was found to be dc-field independent within the uncertainty of the measurements. The coherence times of the Rabi oscillations were similarly consistent at $\sim 1.5\,\mu\mathrm{s}$, and limited by the homogeneity of the probe microwave field across the spatial extent of the cloud of atoms.

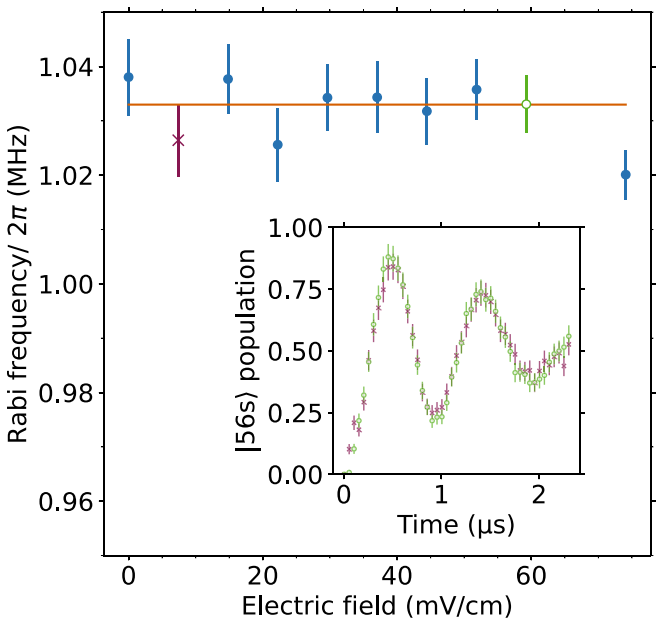

Figure 5. Measurements of the resonant Rabi frequency of the single-color two-photon $|55\mathrm{s}\rangle \rightarrow |56\mathrm{s}\rangle$ transition in the presence of a microwave dressing field for which $\Delta_{\mathrm{null}} = +2\pi \times 10\,\mathrm{MHz}$ and $F_{\mathrm{null}} = 2.78\,\mathrm{mV\,cm^{-1}}$ as determined from the Floquet calculations. The average value of the Rabi frequency is indicated by the horizontal green line. Examples of the experimental data from which the Rabi frequencies were obtained are displayed for the data points represented by the purple cross ($F_{\mathrm{dc}} = 7\,\mathrm{mV\,cm^{-1}}$) and open green circle ($F_{\mathrm{dc}} = 59\,\mathrm{mV\,cm^{-1}}$) in the inset.

4.3. Physical interpretation

The effect of the $|55\mathrm{s}\rangle \rightarrow |55\mathrm{p}\rangle$ dressing field on the $|55\mathrm{s}\rangle \rightarrow |56\mathrm{s}\rangle$ transition can be understood intuitively by considering the $|55\mathrm{s}\rangle$ and $|55\mathrm{p}\rangle$ states as a dressed two-level system [36]. In this system the dressed eigenstates can be expressed as,

$$|1(N)\rangle = \sin\theta\,|55\mathrm{s}, N+1\rangle + \cos\theta\,|55\mathrm{p}, N\rangle \tag{8}$$

$$|2(N)\rangle = \cos\theta\,|55\mathrm{s}, N+1\rangle - \sin\theta\,|55\mathrm{p}, N\rangle, \tag{9}$$

where N is the photon number and the mixing angle, θ, is dependent on the detuning, Δ_{null}, and resonant Rabi frequency, Ω_{null}, of the differential-polarizability-nulling microwave field such that $\tan 2\theta = -\Omega_{\mathrm{null}}/\Delta_{\mathrm{null}}$. The mixing angle is defined between $0 \leqslant 2\theta < \pi$. This reduction is reasonable under the conditions of the experiments because in weak dc fields only the $|55\mathrm{s}\rangle$ and $|55\mathrm{p}\rangle$ states are significantly perturbed by the nulling field. In particular, the nulling field is far off resonance from the $|56\mathrm{s}\rangle \rightarrow |56\mathrm{p}\rangle$ transition, i.e. $\omega_{56\mathrm{s},56\mathrm{p}} - \omega_{\mathrm{null}} \simeq 2\pi \times 0.4\,\mathrm{GHz}$, and as a result the differential polarizability of the $|55\mathrm{s}\rangle$ and $|56\mathrm{s}\rangle$ states is significantly reduced when the polarizability of the dressed state approaches that of the $|56\mathrm{s}\rangle$ state.

Using this simple model, optimal dressing field parameters can be estimated by identifying the appropriate mixing angle from the polarizabilities of the $|55\mathrm{s}\rangle$ $[(\alpha_{55\mathrm{s}} = 2.058\,\mathrm{GHz\,(V\,cm^{-1})^{-2}})]$, $|55\mathrm{p}\rangle$ $[(\alpha_{55\mathrm{p}} = 4.804\,\mathrm{GHz\,(V\,cm^{-1})^{-2}})]$, and $|56\mathrm{s}\rangle$ $[(\alpha_{56\mathrm{s}} = 2.334\,\mathrm{GHz\,(V\,cm^{-1})^{-2}})]$ states, and the dressed-state amplitudes. The dressed state that the atom is initially prepared in depends on the sign of the detuning of the microwave dressing field. For $\Delta_{\mathrm{null}} > 0$, as was the case in the experiments described here, the system is prepared in the $|1(N)\rangle$ state. Under these conditions, the dressing field parameters were calculated using $\alpha_{56\mathrm{s}} = \alpha_{55\mathrm{s}} \sin^2\theta + \alpha_{55\mathrm{p}} \cos^2\theta$ to obtain an optimal mixing angle of $\theta = 1.248\,\mathrm{rad}$ (i.e. $\Omega_{\mathrm{null}}/\Delta_{\mathrm{null}} \simeq 0.752$).

This dressed-state model holds in weak dc fields for which the effective dc and ac Stark effects balance each other. This requires that the Stark shifts of the $|55\mathrm{s}\rangle$ and $|56\mathrm{s}\rangle$ states are purely quadratic, and that the dc Stark shift of the $|55\mathrm{s}\rangle \rightarrow |55\mathrm{p}\rangle$ transition—if considered in isolation—is small compared to the detuning Δ_{null}. This can be seen in figure 6 where the Stark shift of the single-color two-photon $|55\mathrm{s}\rangle \rightarrow |56\mathrm{s}\rangle$ transition in the absence of the nulling field (dotted red curve) is compared to the Stark shift of the same transition in the presence of the optimal nulling field as determined using this model (continuous green curve). In this case, the nulling field had a detuning $\Delta_{\mathrm{null}} = +2\pi \times 10\,\mathrm{MHz}$, and to achieve the optimal value of θ, an amplitude of $2.39\,\mathrm{mV\,cm^{-1}}$. From these data it is seen that the differential polarizability of the $|55\mathrm{s}\rangle$ and $|56\mathrm{s}\rangle$ states is nulled, so that the dc Stark effect remains within $\pm 15\,\mathrm{kHz}$, for dc fields up to

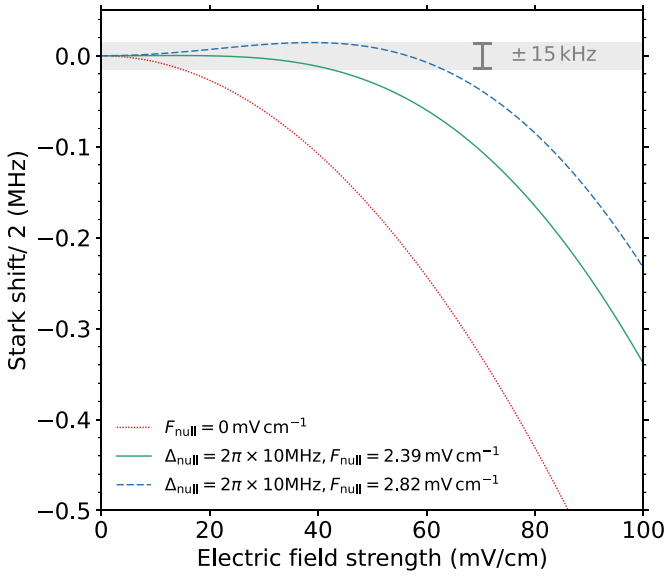

Figure 6. Calculated dc Stark shifts of the single-color two-photon $|55s\rangle \rightarrow |56s\rangle$ transition. The dotted red curve represents the Stark shift in the absence of a nulling microwave field. The continuous green curve is the Stark shift in the presence of such a field with $\Delta_{null} = +2\pi \times 10\,MHz$ and a field strength predicted by the dressed two-level model (see text for details). The dashed blue curve is the transition frequency in the presence of a dressing field for which $\Delta_{null} = +2\pi \times 10\,MHz$ and $F_{null} = 2.82\,mV\,cm^{-1}$, as used in the experiments.

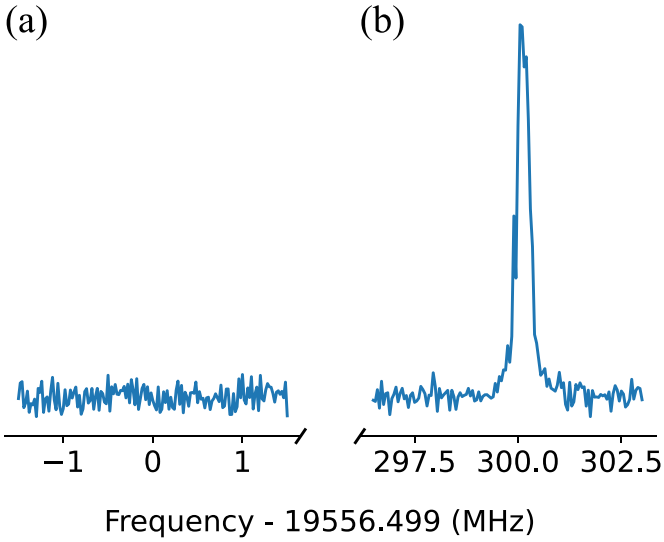

Figure 7. Spectra of (a) the single-color, and (b) the two-color two-photon $|55s\rangle \rightarrow |56s\rangle$ transition driven by a weak probe field in the presence of a strong dressing field at a frequency $\omega_{dress} = \omega_{55s,56s}/2 - 2\pi \times 299.6\,MHz$, where $\omega_{55s,56s}/2 = 2\pi \times 19\,556.499\,MHz$.

$F_{dc} \simeq 40\,mV\,cm^{-1}$. In fields greater than this, the ac and dc Stark shifts no longer compensate each other exactly and the dc Stark shift dominates. However, as can be seen from the dashed blue curve in figure 6, the dc Stark shift can be maintained within $\pm 15\,kHz$ in fields up to $60\,mV\,cm^{-1}$ if F_{null} is increased to $2.82\,mV\,cm^{-1}$. In this case, a positive Stark shift occurs in weak fields before a turning point is encountered at $+15\,kHz$ after which the Stark shift becomes negative.

In general, the range of dc electric fields over which efficient nulling of the differential polarizability of the $|55s\rangle$ and $|56s\rangle$ states is achieved increases with the detuning Δ_{null}. However, as can be inferred from the dependence of θ on the detuning, this comes at the cost of requiring higher Rabi frequencies to admix sufficient $|55p\rangle$ character into the $|55s\rangle$ state and balance the dc Stark effect. For weak nulling fields, the optimal value of Δ_{null} to maximize the range of dc fields over which the polarizability is nulled effectively, depends linearly on F_{null}. For values of F_{null} below $\sim 50\,mV\,cm^{-1}$, this leads to the requirement that $\Delta_{null} = +2\pi \times (3.95\,F_{null})\,MHz\,(mV\,cm^{-1})^{-1}$. The limitation on the maximum usable dressing field amplitude, or dressing field detuning, is imposed by the requirement that the dressing field remains far off resonance from the $|56s\rangle \rightarrow |56d\rangle$ transition at $2\pi \times 11.094\,260\,GHz$ which becomes electric-dipole allowed upon ℓ-mixing in the presence of a dc field. Effects of this additional contribution to the ac Stark shift of the $|55s\rangle \rightarrow |56s\rangle$ transition in the presence of the dressing field become apparent for values of $F_{null} \gtrsim 50\,mV\,cm^{-1}$, and therefore values of $\Delta_{null} \gtrsim 2\pi \times 200\,MHz$. Under these conditions, the linear relationship between these parameters begins to break down.

4.4. Differential polarizability nulling in the presence of a second strong dressing field

In experiments to coherently interface Rydberg He atoms with microwave fields in superconducting CPW resonators, the addition of a polarizability nulling microwave field as described above will allow stronger atom-resonator coupling by reducing the sensitivity of the $|55s\rangle \rightarrow |56s\rangle$ transition to weak residual inhomogeneous stray electric fields and permit smaller atom-surface, or atom-resonator distances where the resonator field is stronger. However, to offer flexibility in the resonator operating temperature, which affects the resonator resonance frequency, and access the single-photon strong coupling regime, it is also desirable to drive the $|55s\rangle \rightarrow |56s\rangle$ transition as a two-color two-photon transition with one photon provided by the resonator and the other by an additional strong microwave dressing field. This can be achieved by detuning the resonator by Δ_{res} from $\omega_{55s,56s}/2$, and introducing a second strong microwave control field detuned by $-\Delta_{res}$ from $\omega_{55s,56s}/2$. In this situation, the frequency of the control field can then be adjusted to tune the transition between the Rydberg states into resonance with the resonator resonance frequency.

To demonstrate this scheme with a strong control field detuned by $\Delta_{ctl} = -2\pi \times 299.6\,MHz$ from $\omega_{55s,56s}/2$, spectra of the two-photon $|55s\rangle \rightarrow |56s\rangle$ transition were recorded with a weak probe field in the frequency ranges within $\pm 1.5\,MHz$ of $\omega_{55s,56s}/2$, and $\omega_{55s,56s}/2 + \Delta_{res}$. These are displayed in figures 7(a) and (b), respectively. Because the output power of the microwave source used to generate the weak probe field was $\sim 28\,dB$ lower than that used when recording the spectra in

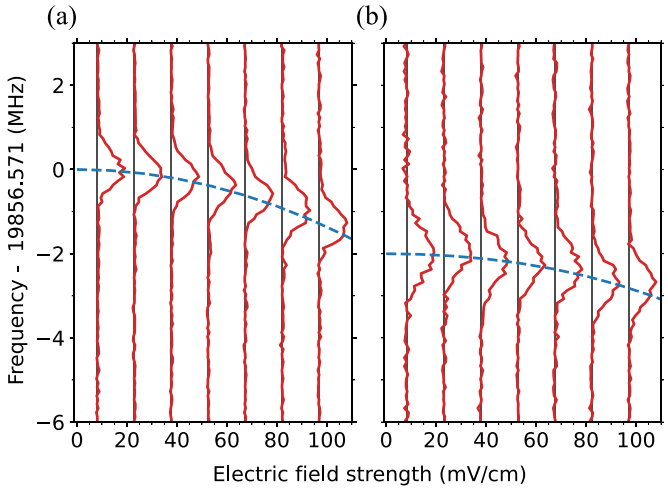

Figure 8. Measured (continuous red curves) and calculated (dashed blue curves) Stark shifts of the two-color two-photon $|55s\rangle \rightarrow |56s\rangle$ transition driven by a weak probe field in the presence of strong control field at a frequency $\omega_{\rm dress} = \omega_{55s,56s}/2 - 2\pi \times 299.6\,{\rm MHz}$. The data were recorded in the (a) absence, and (b) presence of a polarizability-nulling field with a detuning $\Delta_{\rm null} = 2\pi \times 30\,{\rm MHz}$, and amplitude $F_{\rm null} = 6.6\,{\rm mV\,cm^{-1}}$.

figures 3, no population transfer to the $|56s\rangle$ state is seen on the single-color two-photon resonance at $\omega_{55s,56s}/2$ in panel (a). However, the presence of the strong control field does result in population transfer at the two-color two-photon transition frequency, $\omega_{55s,56s}/2 + \Delta_{\rm res}$, in panel (b). On this resonance, the atoms absorb one photon from the weak probe field and one from the strong control field. In the hybrid cavity quantum electrodynamics (QED) setting, the weak probe field would be supplied by the resonator field.

The strong control field applied to drive the two-color two-photon $|55s\rangle \rightarrow |56s\rangle$ transition in figure 7(b) causes an ac Stark shift, but does not preclude the addition of a further polarizability-nulling microwave field to minimize the dc Stark shift of the transition. This can be seen from the data in figure 8. The Stark shift of the two-color two-photon transition recorded by scanning the frequency of the weak probe field in the presence of the strong control field without polarizability nulling is seen in figure 8(a). The measured spectral lines have FWHM of ∼920 kHz. This corresponds to the Fourier transform limit of the $T_\mu = 1$-μs-duration microwave pulses. These spectral lines are broader than the features in figure 3 because of the shorter interrogation time, which was necessary to minimize effects of inhomogeneities in the two strong control and nulling microwave fields. They were also measured at the single-photon level, rather than the two-photon level. From these data, in the absence of the polarizability nulling field the Stark shift of the two-color two-photon transition remains below 460 kHz i.e. half of the FWHM, for dc fields below $\sim 55\,{\rm mV\,cm^{-1}}$. The application of the polarizability nulling field, with $\Delta_{\rm null} = +2\pi \times 30\,{\rm MHz}$ and $F_{\rm null} = 6.6\,{\rm mV\,cm^{-1}}$ (figure 8(b)) causes an ac Stark shift of -483 kHz, and a concomitant reduction in the differential polarizability of the $|55s\rangle$ and $|56s\rangle$ states. Under these conditions, the dc Stark shift of transition remains below 460 kHz for fields up to $\sim 75\,{\rm mV\,cm^{-1}}$.

The data in figure 8 demonstrate that a two-color two-photon transition between $|ns\rangle$ and $|(n+1)s\rangle$ Rydberg states in He can be exploited to allow tunable absorption of single photons from a weak probe field, while simultaneously applying a strong microwave field detuned from the $|ns\rangle \rightarrow |np\rangle$ transition to null the differential polarizability of these states. The range of dc electric fields over which nulling is demonstrated in figure 8(b) is compatible with those encountered in experiments with He Rydberg atoms coupled to superconducting circuits. However, this could be extended through the use of stronger nulling field strengths with larger detuings. These could be achieved using a higher power microwave source, or improving the propagation efficiency of the microwave radiation into the measurement region of the experimental apparatus. To maximize the effectiveness of the nulling and control fields, it is essential to ensure that they are both homogeneous across the volume covered by the Rydberg atoms. The interrogation time, and hence spectral line-widths, in the experiments reported here were limited by the variation in the strength of these fields with position across the bunch of excited Rydberg atoms. In the future, this limitation can be addressed through the use of more slowly moving beams of atoms, or atoms confined in traps.

5. Discussion and conclusion

We have shown experimentally, and with the aid of numerical calculations that off-resonant microwave dressing fields can be used to engineer two-photon $|ns\rangle \rightarrow |(n+1)s\rangle$ Rydberg–Rydberg transitions between triplet states in He, such that the differential static electric dipole polarizability of these states, and hence the dc Stark shift of the transition between them is effectively eliminated for dc fields up to $\pm 60\,{\rm mV\,cm^{-1}}$. This can be interpreted physically, and appropriate dressing field detunings and amplitudes estimated using a simple model that accounts for the static electric dipole polarizabilities of the dressed states. A complete numerical treatment, using the Floquet method and matrix diagonalization, yielded calculated Stark shifts in excellent quantitative agreement with the experimental data.

The Rydberg states considered here have already been successfully used in experiments to coherently couple Rydberg atoms to microwave fields in chip-based superconducting microwave resonators. They are therefore of particular interest in ongoing research directed toward the refinement and further development of hybrid interfaces between Rydberg atoms and superconducting microwave circuits. At these interfaces, residual uncancelled stray electric fields impact coherence times and fidelity in state preparation and manipulation. The addition of a further strong control field to supply one of the photons required to drive the $|55s\rangle \rightarrow |56s\rangle$ transition as a two-color two-photon transition, with the second photon provided by a weak probe field allows broadly tuneable Rydberg–Rydberg transitions, with minimal sensitivity

to residual uncancelled dc electric fields to be engineered. This methodology, and the results presented, pave the way toward the single-photon strong-coupling regime of hybrid cavity QED with Rydberg atoms and superconducting circuits.

Data availability statement

All data that support the findings of this study are included within the article (and any supplementary files).

Acknowledgments

This work was supported by the European Research Council (ERC) under the European Union's Horizon 2020 research and innovation program (Grant No. 683341), and the Engineering and Physical Sciences Research Council through the EPSRC Centre for Doctoral Training in Delivering Quantum Technologies (Grant No. EP/S021582/1).

ORCID iD

S D Hogan https://orcid.org/0000-0002-7720-3979

References

[1] Bernien H *et al* 2017 *Nature* **551** 579–84
[2] de Léséleuc S, Lienhard V, Scholl P, Barredo D, Weber S, Lang N, Büchler H P, Lahaye T and Browaeys A 2019 *Science* **365** 775–80
[3] Browaeys A and Lahaye T 2020 *Nat. Phys.* **16** 132–42
[4] Arute F *et al* 2019 *Nature* **574** 505–10
[5] Krinner S *et al* 2022 *Nature* **605** 669–74
[6] Rabl P, DeMille D, Doyle J M, Lukin M D, Schoelkopf R J and Zoller P 2006 *Phys. Rev. Lett.* **97** 033003
[7] Hafezi M, Kim Z, Rolston S L, Orozco L A, Lev B L and Taylor J M 2012 *Phys. Rev.* A **85** 020302(R)
[8] Patton K R and Fischer U R 2013 *Phys. Rev. Lett.* **111** 240504
[9] Pritchard J D, Isaacs J A, Beck M A, McDermott R and Saffman M 2014 *Phys. Rev.* A **89** 010301(R)
[10] Gard B T, Jacobs K, McDermott R and Saffman M 2017 *Phys. Rev.* A **96** 013833
[11] Sárkány L, Fortágh J and Petrosyan D 2018 *Phys. Rev.* A **97** 032341
[12] Petrosyan D, Mølmer K, Fortágh J and Saffman M 2019 *New J. Phys.* **21** 073033
[13] Vogt T, Gross C, Han J, Pal S B, Lam M, Kiffner M and Li W 2019 *Phys. Rev.* A **99** 023832
[14] Hogan S D, Agner J A, Merkt F, Thiele T, Filipp S and Wallraff A 2012 *Phys. Rev. Lett.* **108** 063004
[15] Thiele T, Deiglmayr J, Stammeier M, Agner J A, Schmutz H, Merkt F and Wallraff A 2015 *Phys. Rev.* A **92** 063425
[16] Morgan A A and Hogan S D 2020 *Phys. Rev. Lett.* **124** 193604
[17] Walker D M, Brown L L and Hogan S D 2022 *Phys. Rev.* A **105** 022626
[18] Hattermann H, Mack M, Karlewski F, Jessen F, Cano D and Fortágh J 2012 *Phys. Rev.* A **86** 022511
[19] Hermann-Avigliano C, Teixeira R C, Nguyen T L, Cantat-Moltrecht T, Nogues G, Dotsenko I, Gleyzes S, Raimond J M, Haroche S and Brune M 2014 *Phys. Rev.* A **90** 040502(R)
[20] Kaiser M *et al* 2022 *Phys. Rev. Res.* **4** 013207
[21] Peper M, Deiglmayr J, Merkt F, Sanna C and van den Heuvell H 2019 *Phys. Rev.* A **100** 032512
[22] Mozley J, Hyafil P, Nogues G, Brune M, Raimond J M and Haroche S 2005 *Eur. Phys. J.* D **35** 43–57
[23] Jones L A, Carter J D and Martin J D D 2013 *Phys. Rev.* A **87** 023423
[24] Ni Y, Xu P and Martin J D D 2015 *Phys. Rev.* A **92** 063418
[25] Booth D W, Isaacs J and Saffman M 2018 *Phys. Rev.* A **97** 012515
[26] Walker D M, Morgan A A and Hogan S D 2020 *Appl. Phys. Lett.* **117** 204001
[27] Hogan S D, Houston Y and Wei B 2018 *J. Phys. B: At. Mol. Opt. Phys.* **51** 145002
[28] Zimmerman M L, Littman M G, Kash M M and Kleppner D 1979 *Phys. Rev.* A **20** 2251–75
[29] Shirley J H 1965 *Phys. Rev.* **138** B979–87
[30] Zhelyazkova V and Hogan S 2015 *Mol. Phys.* **113** 3979
[31] Drake G W F 1999 *Phys. Scr.* **T83** 83
[32] Gallagher T F 1994 *Rydberg Atoms* (Cambridge University Press)
[33] Ho T S and Chu S I 1984 *J. Phys. B: At. Mol. Phys.* **17** 2101
[34] Chu S I 1985 Developments in semiclassical Floquet theories for intense-field multiphoton processes *Advances in Atomic and Molecular Physics* vol 21 (Elsevier) pp 197–253
[35] Halfmann T, Koensgen J and Bergmann K 2022 *Meas. Sci. Technol.* **11** 1510–4
[36] Dalibard J and Cohen-Tannoudji C 1985 *J. Opt. Soc. Am.* B **2** 1707–20